

Thank you to both Reviewer #1 and #2 for the thoughtful and constructive comments. Addressing these comments have helped to clarify a number of points in the paper. We have worked to address the comments as completely as possible in the revised manuscript. Point-by-point responses to the comments are below the blue text in black font.

Reviewer #1:

Solomon et al assess the relative impact of CCN and INP perturbations on the cloud properties of Arctic mixed-phase clouds in a numerical study based on observations obtained at Oliktok Point in Alaska for the night of April 16th 2015. The authors identify a range of interesting mechanisms in which the cloud response to the aerosol may be buffered in the mixed-phase regime as opposed to the warm-phase regime. Furthermore, their results show that INP perturbations proved to be more efficient at altering cloud properties than CCN perturbations for the same fractional increase/decrease. The study is well-conceived, well written, of interest to the readership of ACP and deserves publication following minor revisions.

Minor Comments:

1) P1L26: “decrease in CCN and INPs results in an increase in the cloud-top longwave cooling rate”. This statement sounds like the cloud-top cooling rate is getting stronger for a decrease in CCN, which is not the case. I suggest to either refer to it as longwave heating rate at cloud top as done in Fig. 3, or rephrase for clarification.

This sentence is referring to the LinIce0.5 run where a similar fractional decrease in INP and CCN produces and increase in LWP. The sentence has been changed to read “...a run with an equivalent fractional decrease in CCN and INPs results in an increase in the cloud-top longwave cooling rate...”.

2) P3L2: “only a few INPs are needed to glaciatae a cloud”. I would argue this still to be an open question (as the authors discuss in their conclusions). As this is relevant to the paper a brief discussion on this issue with a wider referencing of the excisiting literature may be appropriate here. References that come to mind include:

Loewe et al, ACP, 2017: “Modelling micro- and macrophysical contributors to the dissipation of an Arctic mixed-phase cloud during the Arctic Summer Cloud Ocean Study (ASCOS)”

Stevens et al, ACP, 2018: “A model intercomparison of CCN-limited tenuous clouds in the high Arctic”

This discussion is about INP and the studies about glaciatae due to limited CCN are outside the scope of this study but these results are very interesting and important so we have reworded the last sentence in this paragraph to read, “However, it is important to note that an environment with a few INP per liter or limited CCN can glaciatae a mixed-phase cloud (DeMott et al. 2010; Mauritsen et al. 2011; Loewe et al. 2017; Stevens et al. 2018).”

3) P10L11: “LWP consistent with observations”: From the observations it seems that a considerably thicker MPC develops during the night with LWP reaching 60 g/m² and values above 40g/m² for what seems like ~6h of the night. The LWP in the simulations seems underestimated. Please comment.

Yes, this is the case for the cloud during 16 April. The simulations are being compared to the cloud observed during 17 April, which has LWP less than 30 g/m² and a liquid fraction less than or equal to 50%.

4) The layering of the CCN and INP when a prognostic treatment is used is an interesting finding of this study. Can the authors elaborate why they believe turbulent transport to cause the build-up of CCN above the cloud? Would one not expect turbulent mixing of cloud droplets out of the cloud to be similarly efficient to entrainment of CCN from above into the cloud? It seems unclear to me how turbulence could generate a gradient in number concentration? Please elaborate.

Yes, it is interesting that the increase in CCN due to turbulent transport can exceed the loss due to entrainment. Thank you for pointing out that we need to add more to explain this result. This result is because the resolved cloud-driven eddies mix the aerosols and hydrometeors at cloud top and the subgrid mixing mix the aerosols into the inversion. This subgrid mixing is due to the weak inversion and mixes the CCN above the entrainment zone. We have added these details to the text.

5) Figure 5: What does Ni+N_s look like at cloud top? Would one not expect changes in Ni here due to the decrease in temperature (Fig. 4d). Here the nucleation of new crystals occurs which then get processed and mixed through the cloud. So while there are no changes in number concentration at cloud base, the increased cloud top cooling may drive changes in ice crystal number concentration elsewhere in the cloud?

Within the cloud layer ice crystals are well-mixed so the ice plus snow number concentration is constant and Ni+N_s at cloud top looks very similar to Ni+N_s at cloud base. There are three sources for INP that can nucleate in the cloud; INP that have been entrainment into the cloud layer at cloud top, activation of additional INP bins as temperatures decrease, and INP advected in from below the cloud layer that have been recycled. These INP activate at cloud top so Ni is largest at cloud top and N_s is largest at cloud base.

6) P6L12: Please add for clarification what the remaining pathway for snow formation is in your model? I would assume that only growth of ice crystals by vapour deposition remains?

Yes this is correct. We have added the sentence, “Therefore, snow water content is dependent on vapour deposition, auto-conversion from ice to snow, and sublimation.”

7) The mechanism of CCN and INP changes impacting the LW cloud top cooling rate (even for thick clouds) and the consequent changes in IWP (even for CCN changes only) is very interesting. It had also been found and hypothesised in a different model for a different case by Possner et al. (2017) where an increase in CCN increased cloud-top cooling, which increased the ice crystal number concentration. Ice water mass increased by increased vapour deposition onto the more numerous crystals (similar as to what the authors see in Fig. 7 for their LinIce experiments). While the feedback here manifests itself differently in simulations with CCN seeding only, it is encouraging to see consistency amongst models and different cases where a feedback through cloud-top cooling impacts the ice phase and stabilises the cloud. This may be worth adding to your discussion. Possner et al, GRL, 2017: “Cloud response and feedback processes in stratiform mixedphase clouds perturbed by ship exhaust”

This is very interesting and we thank the reviewer for this comment. In the Summary and discussion section we have added, “Results consistent with this study were found in Possner et al. (2017), which investigated the impact of ship emissions on mixed-phase stratocumulus observed during M-PACE. Possner et al. found increased CCN increased cloud top cooling, which increased ice mass due to vapor deposition, resulting in a decrease in vapor available for droplet formation. These results are consistent with the ConIce simulations, where an increase in CCN caused an increase in ice water content, primarily due to increased vapor deposition.”

8) Figure 9a: Consider adding droplet number concentration profile for LinIce2.0 simulation, which is not shown elsewhere in the manuscript, to show how the prognostic treatment of CCN affects the Nd profile.

Thank you for this comment. We have chosen to add these details to the text instead. In Section 5c we have added, “Cloud droplet concentrations are largest approximately 100 meters above cloud base. At hour 10, the maximum cloud droplet concentration at 650 meters is 330 cm^{-3} . Figure 9a shows that allowing for prognostic CCN causes sharper cloud base and cloud top droplet concentrations.”

Reviewer #2:

I found this paper to be of good quality with significant findings surrounding the relative impact of CCN and INP loadings on the stratocumulus cloud properties. I recommend publication in ACP with minor revisions. Please find some of my thoughts and comments below.

Minor Comments:

- 1) Page 3 line 14: Is this due to less big drops?
Yes, the smaller drops reduce the collision-coalescence and make ice nucleation less efficient.
- 2) Page 3 line 24: ok I think I understand this. The increase in number is due to them not freezing and being removed from the cloud?
Yes, this is a correct understanding of the Cziczo et al. (2009), Sullivan et al. (2010), Girard and Sokhandan (2014) studies.
- 3) Page 3 paragraph 3: I think this could benefit from some discussion of secondary ice particle production mechanisms here even though they aren't particularly relevant to the temperature range in this study.
We appreciate this comment but have chosen to leave the text unchanged since adding this discussion would take the focus away from the main points of this study.
- 4) Page 10 line 19: Evaporated within 200 m of cloud base. ‘below cloud base’ should be stated.
Text changed as suggested.
- 5) Page 11 paragraph 1: I found this interesting. A fine balance indeed!

This is very interesting and will be a focus of our future work.

- 6) Page 12 line 13: A reduction in sublimation causes more ice to fall out. Why is sublimation varied in this simulation? Reduced sublimation due to the moistening of the layer below the cloud?

Yes, this is correct. Increased CCN causes larger ice water content due to increased vapor deposition which moistens the air as ice sublimates below the cloud-driven mixed layer. This causes more ice (INP) to fall to the ground and become unavailable for recycling.

- 7) Page 14 line 3. This is interesting that you see larger CCN concentrations above the liquid layer in the inversion. Some observations have found an ultra-clean layer above the cloud top. Could you comment on why you might see something different in this case?

The efficacy of these processes is dependent on the strength of the inversion. Stronger stratification in the inversion would limit the mixing from the cloud layer into the inversion. In this Section we have added, “This turbulent transport is due to both resolved cloud-driven eddies, which mix the aerosols and hydrometeors to cloud top, and unresolved subgrid mixing, which mixes the aerosols into the inversion away from entrainment. This subgrid mixing into the inversion is due to the weak inversion at cloud top.”

- 8) Page 14 line 6. Another interesting finding regarding the location of elevated layer of INP lower in the cloud. I wonder what the implications of this could be.

We need to investigate this for a range of environmental conditions since the net impact will depend on whether the cloud system is coupled to the surface, the strength of the surface fluxes, whether the cloud system is rising or lowering, the strength and humidity of the inversion, whether shortwave radiation is significant, etc.

- 9) Page 15 line 23 the model physics vs the Morrison study could be of key importance.

Yes, this is clearly important. We will definitely look into this in detail in follow-on studies.

- 10) The clouds are clearly very sensitive to the ice phase and how the various processes are treated is crucial. E.g. sublimation, re-circulation, shielding of the ice from the liquid etc. One paper that may be relevant is Abel et al. (2017). They did some modelling that showed how sensitive stratocumulus clouds in Cold Air Outbreaks were to ice phase processes and part of that was the partitioning between the liquid and the ice.

- 11) Page 16: If the cloud becomes coupled to the surface we would lose the reservoir of INP. Why?

In an uncoupled system, there is a reservoir of INP due to sublimation. Coupling causes the cloud-driven mixed layer to be well-mixed all the way to the surface. This causes the reservoir to be mixed into the cloud layer where the INP activate and then fall out of the cloud system.

1 **The relative impact of cloud condensation nuclei and ice nucleating**
2 **particle concentrations on phase-partitioning in Arctic Mixed-Phase**
3 **Stratocumulus Clouds**

4 Amy Solomon^{1,2}, Gijs de Boer^{1,2}, Jessie M. Creamean^{1,2,a}, Allison McComiskey², Matthew
5 D. Shupe^{1,2}, Maximilian Maahn^{1,2}, and Christopher Cox^{1,2}

6 (1) Cooperative Institute for Research in Environmental Sciences, University of Colorado
7 Boulder, Colorado, USA.

8 (2) Earth System Research Laboratory, National Oceanic and Atmospheric Administration,
9 Boulder, Colorado, USA.

10 ^aNow at: Department of Atmospheric Sciences, Colorado State University, Fort Collins,
11 Colorado, USA.

12 Corresponding author: Amy Solomon, NOAA/ESRL, PSD3, 325 Broadway, Boulder,
13 Colorado 80305-3337, USA. (amy.solomon@noaa.gov)

14
15 July 6, 2018, revised Oct 16, 2018

16 Under review ACP

17 **Abstract**

18 This study investigates the interactions between cloud dynamics and aerosols in idealized
19 large-eddy simulations of an Arctic mixed-phase stratocumulus cloud observed at Oliktok
20 Point, Alaska in April 2015. This case was chosen because it allows the cloud to form in
21 response to radiative cooling starting from a cloud-free state, rather than requiring the cloud
22 ice and liquid to adjust to an initial cloudy state. Sensitivity studies are used to identify whether
23 there are buffering feedbacks that limit the impact of aerosol perturbations. The results of this
24 study indicate that perturbations in ice nucleating particles (INPs) dominate over cloud
25 condensation nuclei (CCN) perturbations, i.e., a run with an equivalent fractional decrease in
26 CCN and INPs results in an increase in the cloud-top longwave cooling rate, even though the
27 droplet effective radius increases and the cloud emissivity decreases. The dominant effect of
28 ice in the simulated mixed-phase cloud is a thinning rather than a glaciation, causing the mixed-
29 phase clouds to radiate as a grey body and the radiative properties of the cloud to be more
30 sensitive to aerosol perturbations. It is demonstrated that allowing prognostic CCN and INP
31 causes a layering of the aerosols, with increased concentrations of CCN above cloud top and
32 increased concentrations of INP at the base of the cloud-driven mixed-layer. This layering
33 contributes to the maintenance of the cloud liquid, which drives the dynamics of the cloud
34 system.

1 **1 Introduction**

2 Arctic mixed-phase stratocumulus clouds (AMPS) play a unique role in climate by producing
3 a net warming at the Earth's surface over the annual cycle. This warming is due to the limited
4 amount of incoming solar radiation at high latitudes, causing downward longwave radiative
5 effects to dominate surface cloud forcing in the Arctic. AMPS are characterized by a liquid
6 cloud layer with ice crystals that precipitate from cloud base even at temperatures well below
7 freezing (Hobbs and Rangno, 1998; Intrieri et al., 2002; McFarquhar et al., 2007). The
8 magnitude of the cloud-forced surface warming is primarily a function of the liquid water
9 content of the AMPS and the properties of the cloud droplets (Curry and Ebert, 1992; Curry et
10 al., 1993; Zhang et al., 1996). However, different from warm clouds, the magnitude and
11 properties of cloud liquid in mixed-phase clouds are closely connected to the formation of
12 cloud ice, which limits the availability of water vapor for droplet formation and growth (the
13 Wegener-Bergeron-Findeisen (WBF) mechanism, Wegener, 1911; Bergeron, 1935; Findeisen,
14 1938) and acts as a sink for water vapor through the growth and sedimentation of frozen
15 precipitation.

16 Cloud ice in AMPS must form through heterogeneous nucleation, since temperatures are too
17 warm for homogenous ice nucleation (approximately > 36 °C). Heterogeneous ice nucleation
18 can occur by a number of modes: either in the presence of super-cooled droplets, when an
19 aerosol comes into contact with a droplet (contact freezing), is immersed in a droplet followed
20 by freezing (immersion freezing), or in the absence of droplets through vapor deposition on
21 aerosol (deposition freezing) or liquid forming on aerosol (condensation freezing) (Pruppacher
22 and Klett, 1997). The efficiency of any of these modes in a given environmental state is a
23 function of aerosol properties, which determine whether an aerosol can serve as an ice
24 nucleating particle (INP), cloud condensation nucleus (CCN), or both. Based on measurements
25 from in situ instrumentation and the reduced concentration of ice crystals relative to liquid
26 droplets (Murray et al., 2012), it is believed that only a small fraction of aerosols can serve as
27 INPs. For example, in the Indirect and Semi- Direct Aerosol Campaign (ISDAC) (McFarquhar
28 et al., 2011) that took place off the coast of Utqiagvik, (Barrow) Alaska in the spring of 2008,
29 the number of INPs available were observed to be four orders of magnitude smaller than the
30 number of aerosols serving as CCN. However, it is important to note that an environment with

1 ~~a few INP per liter or limited CCN can glaci~~ate a mixed-phase cloud (DeMott et al., 2010;
2 ~~Mauritsen et al., 2011; Loewe et al., 2017; Stevens et al., 2018).~~

3 The impact of CCN variability on warm cloud structure has been the subject of numerous
4 papers. For a fixed liquid water path (LWP), an increase in CCN in warm clouds will increase
5 the number of droplets and reduce the droplet size. This causes an increase in cloud albedo (the
6 Twomey effect; Twomey, 1977) and potentially suppresses precipitation (the Albrecht effect;
7 Albrecht, 1989). Suppressing precipitation can increase cloud thickness/coverage and cloud-
8 driven turbulence, which increases the entrainment of dry air at cloud top, thereby thinning the
9 cloud (Pincus and Baker, 1994; Stevens et al., 1998). This thinning of the cloud as a response
10 to an increase in aerosols is an example of a buffering feedback that limits the impact of a CCN
11 perturbation on the cloud structure (Stevens and Feingold, 2009). For LWPs greater than
12 approximately 50 gm⁻², AMPS emit as blackbodies (Shupe and Intrieri, 2004) and an increase
13 in CCN has minimal impact on longwave emissivity (Morrison et al., 2008). However, smaller
14 droplets can also reduce the ice water path (IWP) through a reduction in collision-coalescence
15 and riming of snow by droplets (Morrison et al., 2008), as well as, make ice nucleation less
16 efficient (Lance et al., 2011). These are only a few examples of buffering feedbacks that exist
17 in mixed-phase clouds.

18 An increase in INPs in AMPS is known to produce a “glaciation effect”, i.e., a rapid depletion
19 of cloud liquid, in part due to the WBF mechanism and the acceleration of frozen precipitation
20 (Murray et al., 2012). However, the efficacy of this effect is dependent upon the chemical
21 composition of the INPs. In cases where INPs are transported over long distances and coated
22 in sulfate or organic materials, an increased concentration of INPs may actually be linked to a
23 “deactivation effect”. This is because coated particles generally freeze at colder temperatures
24 (Cziczo et al., 2009; Sullivan et al., 2010; Girard and Sokhandan, 2014), changing the number,
25 size and fall speeds of nucleated ice crystals and increasing cloud lifetime. The deactivation
26 effect can cause a significant increase in surface warming, since a decrease in droplet size in
27 optically thin clouds for constant LWP can produce a significant increase in cloud longwave
28 emissivity (Garrett and Zhao, 2006).

- Deleted: only a few
- Deleted: s
- Deleted:
- Deleted: are needed to
- Deleted: (see
- Deleted: discussion in

1 Given the uncertainty in measurements of INPs (DeMott, 2015; Garimella et al., 2017), it has
2 been challenging to study the manifestation of aerosol-cloud interactions in mixed-phase cloud
3 conditions. This study investigates these interactions and their dependence on aerosol
4 partitioning in idealized large-eddy simulations (LES) of an AMPS observed at Oliktok Point,
5 Alaska 5-17Z 17 April 2015. In order to isolate the impact of these interactions on longwave
6 cloud forcing, shortwave radiation is neglected in the simulations. The microphysics used in
7 Solomon et al. (2015) have been modified to include prognostic CCN in addition to prognostic
8 INPs. This allows for a more realistic representation of aerosols advected over the Oliktok
9 Point site. In order to identify aerosol indirect effects in these simulations, aerosol chemistry
10 is specified and, due to the in-cloud temperatures for this case, all cloud ice forms through
11 immersion freezing. The focus on immersion freezing is supported by studies demonstrating
12 that liquid droplets typically form prior to ice formation in mixed-phase cloud environments
13 (e.g. de Boer et al., 2011; Westbrook and Illingworth, 2012).

14 This study is focused on the research questions:

- 15 1) What is the relative impact of CCN versus INP perturbations on the phase partitioning
16 between cloud liquid and cloud ice in AMPS? Specifically, what is the impact on cloud
17 dynamics?
- 18 2) Are there buffering feedbacks in AMPS that limit the impact of CCN/INP
19 perturbations?

20 **2 Case Description**

21 Simulations are set up to recreate conditions observed by the US Department of Energy (DOE)
22 Atmospheric Radiation Measurement (ARM) program third mobile facility (AMF-3) at
23 Oliktok Point, Alaska on and around 17 April 2015 (Figure 1). During this time period, Oliktok
24 Point was situated in a relatively quiet regime synoptically, with surface high pressure to the
25 northwest over the Chukchi Sea, and a weak area of low pressure over central Alaska. This
26 resulted in steadily increasing surface air pressure from around 1008 hPa at 00Z on 16 April
27 to around 1021 hPa at 00Z on 18 April and relatively light ($2-5 \text{ m s}^{-1}$) near-surface winds (U_{10m})
28 from the east-northeast over this entire two-day window (Figures 1f,g). Near-surface air
29 temperatures (T_{2m}) varied dramatically (Figure 1e), depending on time of day and cloud cover,

1 with the coldest temperatures around 250 K during late evening and early morning clear
2 periods on 16 April, and the warmest temperatures being around 258 K during cloudy periods
3 during local night time on 17 April. Near-surface relative humidity (RH_{2m}) showed a weak
4 diurnal signature, ranging from around 80% during local daytime hours and 86-88% during
5 nighttime hours.

6 Radiosonde launches conducted at approximately 2330 UTC on 15 April, 1730 UTC and 2330
7 UTC on 16 April, and 1830 UTC and 2330 UTC on 17 April reveal the evolution of the lower
8 troposphere at Oliktok Point (Figure 1h). The 2330 UTC sounding from 15 April reveals a
9 well-mixed surface layer extending up to around 200 m, a stable layer from 200-700 m and
10 then an elevated layer that is generally well mixed from 700-2000 m. By 1730 UTC a strong
11 inversion formed from 30-300 m above the surface where there is a residual mixed layer from
12 the previous night's cloud cover between 300-600 m. Above this layer, there is a weakly stable
13 layer from 600 m to around 1000 m. A similar vertical structure persists through the rest of
14 the sampling period, with the strength of the near-surface inversion and depth of the overlying
15 mixed layer evolving with time, and general warm-air advection occurring above 1000 m.
16 With the exception of a very dry layer between 200-350 m in the 2330 UTC sounding on 17
17 April, and a saturated layer around 200 m in the 1730 UTC sounding on 16 April, the lower
18 atmosphere (0-700 m) features relative humidity between 70-90%. Above this, RH values
19 feature variability between 30-60%, with the height at which this drop off occurs increasing
20 with time. The last two soundings are substantially drier between 1200-2000 m, with RH
21 values around 20%.

22 On both 16 and 17 April, low-level mixed-phase stratus cloud layers were observed to develop
23 during local night time (~0600-1800 UTC). Surface radiation measurements (Figures 1c,d)
24 clearly demonstrate the presence of these clouds, with the net longwave radiation (LW_{NET})
25 increasing to around 0 W m^{-2} as a result of increased downwelling longwave (LW_{DOWN}) during
26 cloudy periods. An increase in downwelling shortwave radiation may be playing a role in the
27 dissipation of the cloud layer. The presence of cloud is also detected by active remote sensors
28 (Figure 1a), with ceilometer cloud base (black dots) and Ka-band cloud radar reflectivity
29 (colored shading) measurements clearly showing the nighttime appearance of liquid-
30 containing cloud layers between 450 and 700 m (on 16 April) and 800 and 1000 m (on 17

1 April) above the surface, with the cloud on 17 April starting and ending with lower cloud bases
2 and tops. Both radar and surface precipitation gauges indicated weak snowfall associated with
3 these clouds and shortwave irradiance measurements reveal that the surface was snow covered
4 during this time, with surface albedo around 80%.

5 **3 Model Description**

6 Simulations are completed using the large eddy simulation mode of the Advanced Research
7 WRF model (WRFLES) version 3.3.1 (Yamaguchi and Feingold, 2012) with the RRTMG
8 longwave radiation parameterization (Mlawer et al., 1997) and the Morrison two-moment
9 microphysical scheme (Morrison et al., 2009). Collision-coalescence was found to be
10 important in CCN perturbation studies during the Fall 2004 Mixed-Phase Arctic Cloud
11 Experiment (M-PACE; Morrison et al., 2008), however tests with and without riming and
12 collision-coalescence indicated that these processes are not significant for this case and have
13 been neglected in the simulations. Therefore, snow water content is dependent on vapor
14 deposition, auto-conversion from ice to snow, and sublimation. Shortwave radiation is
15 neglected given the nighttime occurrence of these clouds and to be able to focus on longwave
16 indirect aerosol effects. Surface fluxes are calculated using the modified MM5 similarity
17 scheme, which calculates surface exchange coefficients for heat, moisture, and momentum
18 following Webb (1970) and uses Monin–Obukhov with Carlson–Boland viscous sublayer and
19 standard similarity functions following Paulson (1970) and Dyer and Hicks (1970). The land
20 surface is simulated with the unified Noah land-surface model (Tewari et al., 2004). Initial
21 surface pressure is 1020 hPa. The initial surface temperature is 255 K.

22 All simulations are run on a domain of $3.6 \times 3.6 \times 1.4$ km with a horizontal grid spacing of 50
23 m and vertical spacing of 10 m. The domain has $72(x) \times 72(y) \times 140(z)$ grid points and is
24 periodic in both the x and y directions. The top of the domain is at 1.4 km. The model time
25 step is 0.5 seconds.

26 *a. Initial atmospheric profiles*

27 Initial profiles of temperature, moisture and horizontal wind components are based on
28 radiosonde measurements taken at Oliktok Point at 23:30Z 16 April 2015 (Figure 1h).

1 Soundings are not available during the cloudy period (5-18Z), seen in the KAZR reflectivity
2 (Figure 1a). Therefore, the model is initialized with a cloud free sounding and the cloud forms
3 in response to the radiative cooling, rather than starting the stimulation with a “cloudy” profile
4 and requiring the cloud ice and liquid to adjust to the initial state. The potential temperature
5 and water vapor mixing ratio from the radiosonde and the initial profiles used in the simulations
6 are shown in Figure 2. Initial water vapor is increased in the region where cloud liquid water
7 was observed after 5Z in order to produce cloud liquid water at the start of the integration.
8 Initial temperature and subgrid TKE are perturbed below the top of the mixed layer with
9 pseudo-random fluctuations with amplitude of 0.1 K and $0.1 \text{ m}^2 \text{ s}^{-2}$, respectively.

10 ***b. Large-scale forcing***

11 Large-scale subsidence is specified by integrating the prescribed horizontal wind divergence
12 from the surface upward. Divergence is assumed to be equal to $1.8 \times 10^{-6} \text{ s}^{-1}$ below the
13 inversion and zero above, following the Solomon et al. (2015) study. This gives a linear
14 increase in large-scale subsidence from zero at the surface to 1.5 mm s^{-1} at the base of the
15 initial inversion ($z=805 \text{ m}$), above which the large-scale vertical wind is constant. Large-scale
16 subsidence is accounted for via a source term for any prognostic variable other than wind
17 components.

18 Temperature and moisture profiles are nudged to the initial profiles in the top 100 meters of
19 the domain with a time scale of 1 hour. Horizontal winds are nudged to the initial profiles at
20 and below the initial inversion base with a timescale of 2 hours. Nudging of the horizontal
21 wind components, temperature and moisture profiles is performed by adding a source term to
22 the prognostic equations for potential temperature, water vapor, and horizontal wind
23 components.

24 ***c. Droplet number concentration and CCN properties***

25 Because CCN measurements were not available from Oliktok Point during this time, initial
26 CCN size distributions at every gridpoint are based on springtime measurements taken during
27 the ISDAC campaign (Earle et al., 2011). The accumulation mode observed during ISDAC
28 had a concentration of less than 200 cm^{-3} (165 cm^{-3} used in this study), a modal diameter of 0.2

1 microns, and a geometric standard deviation of 1.4. Sensitivity studies vary initial CCN
 2 concentration with an arbitrary multiplication factor C (referred to as the CCN factor). CCN
 3 mean concentration is then treated as a prognostic variable. A prognostic equation for CCN
 4 number concentration has been added to WRFLES,

$$5 \quad \frac{\partial CCN}{\partial t} + ADV + DIFF = \frac{\delta CCN}{\delta t} \Big|_{condensation} + \frac{\delta CCN}{\delta t} \Big|_{evaporation} \quad (1)$$

6 where ADV represents advection and DIFF represents turbulent diffusion. Condensation is a
 7 sink of CCN and evaporation is a source of CCN. Evaporation (condensation) of one droplet
 8 produces (removes) one CCN.

9 Cloud droplets are activated using resolved and subgrid vertical motion (Morrison and Pinto,
 10 2005) and a log-normal aerosol size distribution (assumed to be ammonium bisulfate and 30%
 11 insoluble by volume) to derive cloud condensation nuclei spectra following Abdul-Razzak and
 12 Ghan (2000). As noted in Solomon et al. (2015), because the aerosol number size distribution
 13 peaks at a relatively large diameter of 0.2 microns, the majority of CCN activate into droplets
 14 at low supersaturation (at or below $SS_w = 0.15\%$) for a reasonable range of aerosol composition
 15 assumptions. Since such supersaturations can be generated even by slow updrafts, the
 16 sensitivity of droplet number concentration to aerosol composition is expected to be weak. We
 17 therefore only include simulations that test the sensitivity to mean CCN concentrations.

18 ***d. Ice nucleation***

19 Following Solomon et al. (2015), a prognostic equation for INP number concentration (N_{INP})
 20 has been added to WRFLES,

$$21 \quad \frac{\partial N_{INP}}{\partial t} + ADV + DIFF = \frac{\delta N_{INP}}{\delta t} \Big|_{activation} + \frac{\delta N_{INP}}{\delta t} \Big|_{sublimation} \quad (2)$$

22 where ADV represents advection and DIFF represents turbulent diffusion. Activation is also
 23 referred to as ice nucleation and sublimation represents a source of INP, supporting the
 24 recycling of these particles.

1 Eight prognostic equations are integrated for N_{INP} in equally spaced temperature intervals with
2 nucleation thresholds spanning the range of the in-cloud temperatures (-20.15°C to -14.55°C).
3 Therefore, additional INP become available for activation with decreasing temperature and as
4 the cloud layer cools. INP number concentrations are initially specified at 1.3 L⁻¹ in each bin
5 to produce IWP close to observations for this case. Sensitivity studies vary initial INP
6 concentration with an arbitrary multiplication factor F (referred to as the INP factor).

7 It is assumed that 50% of the INP available in a bin nucleate if the in-situ temperature is below
8 the threshold temperature and the local conditions exceed water saturation. Therefore, initial
9 N_{INP} are a function of the nucleation threshold temperatures and are independent of the in-situ
10 temperature. The in-situ temperature in regions of water saturation determines how many INP
11 are activated. Due to the pristine dendritic nature of the observed crystals and the limited
12 number of INP, ice shattering and aggregation are neglected in the simulations and sublimation
13 returns one INP per sublimated crystal.

14 N_{INP} (in units of L⁻¹) integrated over the domain in each temperature bin k at time t is equal
15 to

$$16 \quad \bar{N}_{INP}(k, t) = \iiint N_{INP}(x, y, z, k, t) \, dx \, dy \, dz. \quad (3)$$

17 Upon sublimation, the modification of activation thresholds that can occur for previously
18 nucleated INP, i.e. preactivation (Roberts and Hallett, 1967), is not considered and N_{INP} are
19 returned to each bin k with weighting

$$20 \quad W_k = [\bar{N}_{INP}(k, 0) - \bar{N}_{INP}(k, t)] / \bar{N}_{INP}(k, 0) \quad (4)$$

21 where W_k is normalized such that $\sum W_k = 1$. The W_k are recalculated each time step. In this
22 way, INP are recycled preferentially to each of the eight temperature bins from which they
23 originated (Feingold et al., 1996).

24 **4 Simulations Completed**

1 Simulations completed for this study are listed in Table 1. A simulation with INP and CCN
2 factors equal to 1.0 is referred to as the Control. To isolate the impact of CCN perturbations
3 on mixed-phase clouds without a change in ice formation, three simulations were run with
4 CCN factors 1/2, 1, 2 and INP factors equal to 1.0 (runs ConIce0.5, Control, ConIce2.0). To
5 identify the impact of CCN perturbations on mixed-phase clouds when ice formation is a linear
6 function of the CCN number concentration, two runs were done with INP and CCN factors
7 equal to 2, one with fixed CCN (FixedCCN2.0) and one with prognostic CCN (LinIce2.0), and
8 one run with INP and CCN factors equal to 1/2 (LinIce0.5).

9 **5 Model Results**

10 *a. Control simulation*

11 The control simulation (CCN and INP factors equal to one) has IWP and LWP consistent with
12 observations on 17 April 2015 (Figures 1b and 3a), and a cloud system that reaches a steady
13 state after 5 hours with liquid water fractions close to 0.5. The cloud-driven mixed-layer depth
14 slowly increases over the 16-hour integration, with both cloud top rising and cloud base
15 lowering at a rate of ~ 5 m/hour. However, the cloud system remains decoupled from the
16 surface layer and a surface inversion of ~ 180 meters in depth is maintained throughout the
17 integration.

18 Rain forms in the liquid layer (with concentrations less than 0.02 cm^{-3}) and evaporates ~~from~~
19 ~~cloud base to~~ 200 meters ~~below~~ cloud base. Therefore, the production and impact of rain on
20 this simulation can be neglected. This is true for the sensitivity studies discussed below as well
21 but would not be the case for runs with more limited CCN, which would produce significant
22 precipitation.

23 Snow does reach the surface during the steady state with a relatively constant flux of $6 \times 10^{-4} \text{ g}$
24 $\text{m}^{-2} \text{ s}^{-1}$. Sublimation at the base of the cloud-driven mixed-layer reduces the snow water content
25 by $6 \times 10^{-6} \text{ g m}^{-3} \text{ s}^{-1}$. In terms of number concentration, this causes the recycling of
26 approximately $1 \text{ L}^{-1} \text{ hour}^{-1}$ of INP back into the cloud-driven mixed-layer. Since total ice
27 crystal number concentrations are $1\text{-}2 \text{ L}^{-1}$ in the mixed-layer over the integration, this indicates
28 that recycling of INP is playing a significant role in the maintenance of cloud ice in this cloud

Deleted: within

Deleted: of

1 system (e.g., Solomon et al., 2015).

2 While the cloud system is maintaining a steady state in cloud ice and liquid, longwave cooling
3 continually cools the cloud-driven mixed-layer, contributing to the maintenance of the phase-
4 partitioning by increased activation of INP within the liquid cloud layer and depletion of water
5 vapor within the mixed-layer. This cooling is required to maintain the cloud liquid because of
6 the continuous depletion of water vapor, and to maintain the cloud ice, since $\sim 2 \text{ L}^{-1}$ of INP are
7 lost to the surface through precipitation each hour.

8 ***b. Impact of CCN perturbations with constant ice formation***

9 The first set of simulations completed for this study tests the sensitivity of the cloud to
10 perturbations in CCN concentrations, while keeping INP concentrations fixed (ConIce
11 simulations). Simulations involved increasing and decreasing the initial CCN concentrations
12 by a factor of two. These runs provide insight into the impact of CCN perturbations in an Arctic
13 environment with stable stratification near the surface and a weak inversion at cloud top with
14 relatively moist air. Figure 3a shows that increasing the CCN concentrations has the expected
15 effect at the beginning of the integrations when the cloud layer is optically thin-- smaller
16 droplets increase the cloud emissivity and thereby longwave cooling at cloud top, increasing
17 turbulence, supersaturation, and droplet formation. The opposite result is found with
18 decreasing CCN concentrations. For these optically thin cases, radiative cooling is a
19 contribution from the full physical depth of the cloud and the increased cooling rate is therefore
20 an expression of increased total emission of the cloud. Figure 3b shows that this also results in
21 faster vapor deposition rates, resulting in increased ice mass given an increase in CCN.
22 However, this increase in IWP plateaus and slowly decreases after hours 5-6 as ice crystals fall
23 out of the cloud layer and are lost from the system. Decreasing CCN results in slower
24 deposition rates and reduced IWP.

25 What is unexpected is that the minimum longwave heating rate (or maximum cooling rate) is
26 not exclusively a function of LWP, even after the clouds become optically thick (Figure 3c).
27 The larger longwave cooling rate associated with a cloud forming in conjunction with elevated
28 CCN concentrations causes increased total water in the cloud-driven mixed-layer (indicating
29 that liquid water increases faster than ice mass), which increases the water vapor mixing ratio

1 below the liquid layer, increasing relative humidity in the mixed-layer below the liquid layer
2 (see Figure 4a). The IWP shows larger temporal variability than the LWP, potentially due to
3 larger sensitivity to small perturbations in relative humidity.

4 Increasing CCN causes the cloud top to rise and the cloud base to lower faster while keeping
5 the maximum buoyancy relatively unchanged, the maximum buoyancy as a function of LWP
6 is similar for ConIce2.0 and Control, with Control approximately 1×10^{-4} less than ConIce2.0
7 for LWP less than 17 gm^{-2} (Figure 3d). The deepening of the cloud layer for an increase in
8 CCN causes the impact of CCN on maximum droplet size to persist throughout the integration
9 (Figure 5a), even though LWP is increasing more rapidly (Figure 3a).

10 The ConIce set of simulations was designed to identify the impact of CCN variability on phase-
11 partitioning and cloud dynamics for a relatively constant magnitude of cloud ice number
12 concentration. This is seen to be the case in Figure 5c, however, interestingly, processes such
13 as sublimation cause ConIce2.0 to have less total cloud ice number concentration than the other
14 two runs (see Figure 4a-d), since a reduction in sublimation causes more INP to fall out of the
15 mixed-layer and less recycling of INP in the cloud layer. However, the differences in relative
16 humidity also play a role here and therefore the sublimation rate is not just a function of the
17 ice present. Increasing CCN causes more rapid mixed-layer cooling (Figure 4b and 5b) and
18 deeper mixed-layer depths, and therefore larger net deposition rates (Figure 5d) and larger
19 IWPs (Figure 3b).

20 *c. Impact of CCN perturbations with linear ice formation*

21 A second set of simulations was completed adding an additional degree of realism to the
22 simulations by scaling INP concentrations with the CCN concentration, i.e., equal INP and
23 CCN factors (LinIce simulations). This was done in order to represent the case of a polluted
24 air mass with equal relative increases of CCN and INP. The fraction of INP to CCN evolves
25 in time as cloud ice forms and precipitates, sublimates below the cloud base, and advects back
26 into the cloud layer with the cloud-driven vertical motions.

27 Figure 6 shows the sensitivity of the LWP and IWP to an increase and decrease in CCN and
28 INP by a factor of 2. Similar to the ConIce runs, the increase in LWP begins to slow when IWP

1 exceeds 20 g m^{-2} . Before hour 5 the ConIce and LinIce runs have similar trajectories. After
2 hour 5 these runs diverge; decreasing CCN and INP factors in LinIce results in larger LWP
3 because of the dominating effect of INP variability on water vapor availability. Increasing
4 CCN and INP factors from 0.5 to 1.0 results in a 63% decrease in LWP at hour 15.

5 The LinIce runs highlight the extreme sensitivity of phase-partitioning between cloud liquid
6 and ice to very small changes in INP concentrations. For these simulations, there are 5 orders
7 of magnitude difference between CCN and INP concentrations, with the scaling done on a
8 percentage basis relative to the absolute amount. In other words, a change in INP from 1 to 2
9 L^{-1} has a substantially larger effect on cloud phase than a change in CCN from 10,000 to 20,000
10 L^{-1} , despite the latter change obviously being much more extreme from the perspective of
11 aerosol number concentration. The CCN variability in the LinIce runs cause a 50% increase in
12 droplet effective radius for a decrease in CCN by a factor of two (Figure 7a). These changes
13 are of the same sign as the ConIce runs but are larger due to the additional impact of INP
14 variability on water vapor available for condensation. Similarly, the reduction of cloud droplet
15 size related to the presence of elevated aerosol concentrations is exacerbated when both INP
16 and CCN concentrations increase due to the combination of more nucleated droplets (on CCN)
17 and increased water vapor deposition (on ice crystals generated by the elevated INP
18 concentrations). However, the impact of the changes in droplet effective radius are small
19 relative to the impact of INP variability on the dynamics of the cloud-driven mixed layer after
20 approximately hour 4. For example, after hour 7 the LinIce0.5 run has a colder cloud-driven
21 mixed-layer than the Control and LinIce2.0 runs (Figure 7b), whereas ConIce2.0 had a colder
22 cloud-driven mixed-layer than ConIce0.5 (Figure 5b).

23 The ratio of INP among the LinIce runs stays relatively constant for the 16-hour integrations
24 (Figure 7c), indicating that differences in sublimation (INP recycling) and ice fall speeds do
25 not produce appreciably different ice crystal number concentrations in the cloud-driven mixed-
26 layer. However, larger deposition rates in the cloud-driven mixed-layer due to increased ice
27 number concentrations (Figure 7d) result in larger ice water mixing ratios (a 31% increase
28 between ConIce2.0 and LinIce2.0), even though mixed-layer temperatures are warmer for an
29 increase in CCN and INP factors, indicating that NDEPS is dominant relative to ice number in
30 controlling IWP.

1 Allowing both prognostic CCN and INP reveals interesting layering of aerosol distributions
2 that results from differential liquid and ice processes. This is seen in Figure 8, where the
3 turbulent advection of droplets into the cloud top inversion causes larger CCN concentrations
4 above the liquid cloud layer than below (Figure 8a). This turbulent transport is due to both
5 resolved cloud-driven eddies, which mix the aerosols and hydrometeors to cloud top, and
6 unresolved subgrid mixing, which mixes the aerosols into the inversion away from
7 entrainment. This subgrid mixing into the inversion is due to the weak inversion at cloud top.
8 The opposite result is found for INP, where gravitational settling of ice crystals and the
9 subsequent sub-cloud sublimation produces locally-elevated INP concentrations in the lowest
10 200 meters (Figure 8b). This layering of aerosols causes larger entrainment of CCN at cloud
11 top and larger entrainment of INP at mixed-layer base as the mixed-layer deepens. As was
12 demonstrated in Solomon et al (2015), the increase in INP at the base of the mixed-layer
13 contributed to the maintenance of the phase-partitioning by making more INP available for
14 activation as ice crystals as the mixed-layer deepens.

15 This layering of aerosols, with increased CCN above the liquid layer and increased INP below
16 the cloud-driven mixed-layer, causes interesting differences between runs with and without
17 prognostic CCN (Figure 9). Cloud droplet concentrations are largest approximately 100 meters
18 above cloud base. At hour 10, the maximum cloud droplet concentration at 650 meters is 330
19 cm⁻³. Figure 9a shows that allowing for prognostic CCN causes sharper cloud base and cloud
20 top droplet concentrations. The increase in CCN above the liquid layer causes increased
21 entrainment of CCN at cloud top (Figure 9a), decreasing the droplet effective radius, increasing
22 the longwave cooling (Figure 9b), increasing the deposition rate and ice water mixing ratio
23 (Figure 9c). Ultimately, these differences result in stronger buoyancy with the cloud layer
24 (Figure 9d), where buoyancy is increased by up to 10%.

25 **6 Summary and Discussion**

26 In this study we use idealized large-eddy simulations to quantify the relative impact of CCN
27 and INP perturbations on the phase-partitioning and dynamics of AMPS. The modeling
28 framework developed in Solomon et al. (2015) to study the recycling of INP has been extended
29 to include prognostic CCN. The first set of simulations were designed to investigate the impact

Formatted: Superscript

1 of relatively small perturbations in CCN compared to studies such as Morrison et al. (2008)
2 and Kravitz et al. (2014) in mixed-phase conditions with essentially constant INP on phase-
3 partitioning and cloud dynamics. It is found that increasing CCN by a factor of two increases
4 LWP by 60-100%, while decreases CCN by a factor of two reduces LWP by less than 8%, i.e.,
5 the impact is highly non-linear. This change stems primarily from an increase in cloud
6 longwave emissivity and associated increase of cloud-top cooling rates, connected to a
7 decrease in droplet size. This elevated cooling rate causes the cloud-driven mixed-layer to
8 cool and deepen more rapidly. However, interestingly, this difference persists even when the
9 cloud radiates as a blackbody, highlighting the influence of early changes to the system.
10 Results consistent with this study were found in Possner et al. (2017), which investigated the
11 impact of ship emissions on mixed-phase stratocumulus observed during M-PACE. Possner et
12 al. found increased CCN increased cloud top cooling, which increased ice mass due to vapor
13 deposition, resulting in a decrease in vapor available for droplet formation. These results are
14 consistent with the ConIce simulations, where an increase in CCN caused an increase in ice
15 water content, primarily due to increased vapor deposition.

16 The sensitivity to CCN in this study is significantly larger than that found in the M-PACE case
17 study by Morrison et al. (2008) and the ISDAC case study by Kravitz et al. (2014). The M-
18 PACE and ISDAC case studies are useful as examples of the extreme range of conditions under
19 which mixed-phase clouds exist. M-PACE took place in October over open water with large
20 fluxes of heat and momentum from the surface into the cloud layer, while ISDAC took place
21 during the spring when the Arctic Ocean was essentially ice-covered and the cloud layer was
22 decoupled from the surface layer.

23 In the M-PACE case study increasing CCN by a factor of 5-6 resulted in an increase in LWP
24 by 20% and a decrease in IWP by 60%. In the ISDAC case study, increasing CCN by a factor
25 of 4 resulted in similar LWP and IWP until hour 12 when the more pristine cloud collapsed. A
26 very interesting difference between this study and the two previous studies is that both the M-
27 PACE and ISDAC studies found IWP to decrease when CCN was increased, while this study
28 finds an increase in IWP due to increased longwave cooling and larger deposition rates. For
29 the ISDAC case study this may be due to the continuous decrease in droplet number
30 concentration, which would cause the cloud dynamics to spin down. This study also finds a

1 significantly larger sensitivity to INP than the M-PACE case study. The M-PACE case study
2 found that a 10X increase in INP resulted in a 120% increase in IWP and a 23% decrease in
3 LWP, while this study finds increasing INP by 2X results in a 60% increase in IWP and a 36%
4 decrease in LWP. These differences need to be investigated further to identify the relative
5 impact of different environmental conditions and model physics.

6 The differences between this study and the M-PACE and ISDAC studies are due in part to the
7 different environmental conditions but the different sensitivities to both CCN and INP are also
8 due to the different parameterizations used in these models. Both the M-PACE and ISDAC
9 studies essentially hold INP fixed, while this study does not constrain INP other than specifying
10 an initial value. This allows for the vertical redistribution of particles throughout the domain,
11 resulting in feedbacks between ice and droplet properties and cloud dynamics not included in
12 the two previous case studies and in many climate and weather-scale models.

13 Additionally, the inclusion of prognostic CCN and INP reveals a number of feedbacks that
14 buffer the cloud system from collapsing. The first buffering feedback is the recycling of INP,
15 which was the focus of the Solomon et al. (2015) study. The IWP, and therefore phase-
16 partitioning between cloud ice and liquid, cannot be maintained without this feedback.
17 However, the reservoir of INP below the mixed-layer would be depleted if cloud-driven mixed-
18 layer became coupled to the surface layer. The second interesting buffering feedback is the
19 layering of the aerosols, with increased concentrations of CCN above cloud top and increased
20 concentrations of INP at the base of the mixed-layer. As demonstrated in this paper, this
21 layering contributes to the maintenance of the cloud liquid, which ultimately drives the
22 dynamics of the cloud system. A third buffering feedback is the thinning of the liquid layer
23 when INP concentrations are increased. The occurrence of this thinning does not produce
24 complete glaciation, rather causes the mixed-phase clouds to radiate as grey bodies and the
25 radiative properties of the clouds to be more sensitive to aerosol perturbations.

26 Ultimately, enhanced observations of the vertical structure of cloud microphysics and aerosol
27 properties are required. Recent work by the DOE ARM program to operate unmanned aircraft
28 and tethered balloons has provided new perspectives on these quantities and the dynamic and
29 thermodynamic conditions supporting these cloud systems (de Boer et al., 2018). Such

1 observational efforts should continue to be pursued further to help constrain the sensitivities
2 demonstrated by numerical studies as presented here.

3 **7 Acknowledgments**

4 This research was supported by the US Department of Energy (DOE) Atmospheric Systems
5 Research (ASR) program (DE-SC0013306) and the National Oceanic and Atmospheric
6 Administration (NOAA) Physical Sciences Division (PSD). Additionally, measurements used
7 in this study were supported by the US Department of Energy Atmospheric Radiation
8 Measurement (ARM) program. [Thank you to Graham Feingold for constructive comments.](#)

1 **8 References**

- 2 Abdul-Razzak, H., and Ghan, S. J.: A parameterization of aerosol activation 2. Multiple aerosol
3 types, *J. Geophys. Res.*, **105**, 6837–6844, 2000.
- 4 Albrecht, B. A.: Aerosols, cloud microphysics, and fractional cloudiness, *Science*, **245**, 1227–
5 1230, 1989.
- 6 Bergeron, T.: in *Proces Verbaux de l'Association de Meteorologie* (ed. Duport, P.) 156-178
7 (International Union of Geodesy and Geophysics, 1935).
- 8 Cziczo, D., Froyd, K., Gallavardin, S., Moehler, O., Benz, S., Saathoff, H., and Murphy, D.:
9 Deactivation of ice nuclei due to atmospherically relevant surface coatings, *Environ.*
10 *Res. Lett.*, **4**:044013, doi:10.1088/1748-9326/4/4/044013, 2009.
- 11 Curry, J. A., and Ebert, E. E.: Annual cycle of radiation fluxes over the Arctic Ocean:
12 Sensitivity to cloud optical properties. *J. Climate.*, **5**, 1267-1280, 1992.
- 13 Curry, J. A., Schramm, J. L., and Ebert, E. E.: Impact of clouds on the surface radiation balance
14 of the ocean, *Meteor. Atmos. Phys.*, **51**, 197-217, 1993.
- 15 de Boer, G., and co-authors: A bird's-eye view: Development of an operational ARM
16 unmanned aerial capability for atmospheric research in Arctic Alaska, *Bull. Amer.*
17 *Meteor. Soc.*, early online release, 2018.
- 18 de Boer, G., Morrison, H., Hildner, R., and Shupe, M. D.: Evidence of liquid-dependent ice
19 nucleation in high-latitude stratiform clouds from surface remote sensors, *Geophys.*
20 *Res. Lett.*, **38**, L01803, 2011.
- 21 DeMott, P. J.: An exploratory study of ice nucleation by soot aerosols, *J. Appl. Meteorol.*,
22 **29**(10), 1072–1079, 1990.
- 23 DeMott, P. J., Prenni, A. J., Liu, X., Petters, M. D., Twohy, C. H., Richardson, M. S.,
24 Eidhammer, T., Kreidenweis, S. M., and Rogers, D. C.: Predicting global atmospheric ice
25 nuclei distributions and their impacts on climate, *P. Natl. Acad. Sci.*, **107**, 11217-11222,
26 doi:10.1073/pnas.0910818107, 2010.
- 27 DeMott, P. J., Prenni, A. J., McMeeking, G. R., Sullivan, R. C., Petters, M. D., Tobo, Y.,
28 Niemand, M., Möhler, O., Snider, J. R., Wang, Z., and Kreidenweis, S. M.: Integrating
29 laboratory and field data to quantify the immersion freezing ice nucleation activity of
30 mineral dust particles, *Atmos. Chem. Phys.*, **15**, 393-409, doi:10.5194/acp-15-393-
31 2015, 2015.

1 Dyer, A. J., and Hicks, B. B.: Flux-gradient relationships in the constant flux layer, *Q. J. Roy.*
 2 *Meteor. Soc.*, **96**, 715–721, 1970.

3 Earle, M. E., Liu, P. S., Strapp, J. W., Zelenyuk, A., Imre, D., McFarquhar, G. M., Shantz, N.
 4 C., and Leitch, W. R.: Factors influencing the microphysics and radiative properties of
 5 liquid-dominated Arctic clouds: Insight from observations of aerosol and clouds during
 6 ISDAC, *J. Geophys. Res. – Atmos.*, **116**, D00T09, 10.1029/2011jd015887, 2011.

7 Feingold, G., Kreidenweis, S. M., Stevens, B., and Cotton, W. R.: Numerical simulation of
 8 stratocumulus processing of cloud condensation nuclei through collision-coalescence, *J.*
 9 *Geophys. Res.*, **101**, 21,391-21,402, 1996.

10 Findeisen, W.: *Kolloid-Meteorologische* 2nd edn (American Meteorological Society, 1938).

11 Garimella, S., Rothenberg, D. A., Wolf, M. J., David, R. O., Kanji, Z. A., Wang, C., Roesch,
 12 M., and Cziczó, D. J.: Uncertainty in counting ice nucleating particles with continuous
 13 diffusion flow chambers, *Atmos. Chem. Phys.*, doi:10.5194/acp-2016-1180, 2017.

14 Garrett, T., and Zhao, C.: Increased Arctic cloud longwave emissivity associated with
 15 pollution from mid-latitudes. *Nature*, **440**, 787–789, 2006.

16 Garrett, T. J., Radke, L. F., and Hobbs, P. V.: Aerosol effects on cloud emissivity and surface
 17 longwave heating in the Arctic, *J. Atmos. Sci.*, **59**, 769-778, 2002.

18 Girard, E., and Sokhandan, A. N.: Relative importance of acid coating on ice nuclei in the
 19 deposition and contact modes for wintertime Arctic clouds and radiation. *Meteorol. Atmos.*
 20 *Phys.*, **123**(1):81-92, 2014.

21 Hobbs, P., and Rangno, A.: Microstructures of low and middle-level clouds over the Beaufort
 22 Sea. *Q. J. Roy. Meteor. Soc.* **124**, 2035–2071, 1998.

23 Intrieri, J. M., Shupe, M. D., Uttal, T., and McCarty, B. J.: An annual cycle of Arctic cloud
 24 characteristics observed by radar and lidar at SHEBA, *J. Geophys. Res.*, **107**, 8030,
 25 doi:10.1029/ 2000JC000423, 2002.

26 Lance, S., Shupe, M. D., Feingold, G., Brock, C. A., Cozic, J., Holloway, J. S., Moore, R. H.,
 27 Nenes, A., Schwarz, J. P., Spackman, J. R., Froyd, K. D., Murphy, D. M., Brioude, J.,
 28 Cooper, O. R., Stohl, A., and Burkhart, J. F.: Cloud condensation nuclei as a modulator
 29 of ice processes in Arctic mixed-phase clouds, *Atmos. Chem. Phys.*, **11**, 8003-8015,
 30 <https://doi.org/10.5194/acp-11-8003-2011>.

Formatted: Indent: Left: 0", Hanging: 0.5"

Deleted: ¶

Deleted: ¶

Formatted: Justified, Indent: Left: 0", Hanging: 0.5", Line spacing: 1.5 lines

Deleted: ¶

Formatted: Font: 12 pt

1 [Loewe, K., Ekman, A. M. L., Paukert, M., Sedlar, J., Tjernström, M., and Hoose, C.: Modelling](#)
2 [micro- and macrophysical contributors to the dissipation of an Arctic mixed-phase](#)
3 [cloud during the Arctic Summer Cloud Ocean Study \(ASCOS\), *Atmos. Chem. Phys.*,](#)
4 [17, 6693-6704, <https://doi.org/10.5194/acp-17-6693-2017>, 2017.](#)

5 [Mauritsen, T., Sedlar, J., Tjernström, M., Leck, C., Martin, M., Shupe, M., Sjogren, S., Sierau,](#)
6 [B., Persson, P. O. G., Brooks, I. M., and Swietlicki, E.: An Arctic CCN-limited cloud-](#)
7 [aerosol regime, *Atmos. Chem. Phys.*, 11, 165–173, \[165-2011, 2011.\]\(https://doi.org/10.5194/acp-11-

8 <a href=\)](#)

9 McFarquhar, G. M., Zhang, G., Poellot, M. R., Kok, G. L., McCoy, R., Tooman, T., and
10 Heymsfield, A. J.: Ice properties of single layer stratocumulus during the Mixed-Phase
11 Arctic Cloud Experiment (MPACE). Part I: Observations, *J. Geophys. Res.*, **112**,
12 D24202, doi:10.1029/2007JD008646, 2007.

13 McFarquhar, G., and coauthors.: Indirect and semi-direct aerosol campaign: The impact of
14 Arctic aerosols on clouds, *Bull. Am. Meteorol. Soc.* **92**, 183–201, 2011.

15 Mlawer, E. J., Taubman, S. J., Brown, P. D., Iacono, M. J., and Clough, S. A.: Radiative
16 transfer for inhomogeneous atmospheres: RRTM, a validated correlated-k model for
17 the longwave, *J. Geophys. Res.*, **102**, 16663–16682, 1997.

18 Morrison, H., and Pinto, J. O.: Mesoscale modeling of springtime Arctic mixed-phase
19 stratiform clouds using a new two-moment bulk microphysics scheme, *J. Atmos. Sci.*, **62**,
20 3683-3704, 2005.

21 Morrison, H., Thompson, G., and Tatarskii, V.: Impact of cloud microphysics on the
22 development of trailing stratiform precipitation in a simulated squall line: Comparison of
23 one- and two-moment schemes, *Mon. Wea. Rev.*, **137**, 991-1007,
24 doi:10.1175/2008MWR2556.1, 2009.

25 Morrison, H., Pinto, J. O., Curry, J. A., and McFarquhar, G. M.: Sensitivity of modeled arctic
26 mixed-phase stratocumulus to cloud condensation and ice nuclei over regionally varying
27 surface conditions, *J. Geophys. Res.*, **113**, D05203, doi:10.1029/2007JD008729, 2008.

28 Murray, B. J., O’Sullivan, D., Atkinson, J. D., and Webb, M. E.: Ice nucleation by particles
29 immersed in supercooled cloud droplets, *Chem. Soc. Rev.* **41**, 6519–6554, 2012.

30 Paulson, C. A.: The mathematical representation of wind speed and temperature profiles in the
31 unstable atmospheric surface layer, *J. Appl. Meteor.*, **9**, 857–861, 1970.

Formatted: Font: Times New Roman, 12 pt

Formatted: Font: 12 pt

Formatted: Indent: Left: 0", Hanging: 0.5"

Formatted: Font color: Auto, (Asian) Japanese

1 Pincus, R., and Baker, M.B.: Effect of precipitation on the albedo susceptibility of marine
 2 boundary layer clouds, *Nature*, **372**, 250–252, 1994.

3 ~~Possner, A., Ekman, A. M. L., and Ulrike, L.: Cloud response and feedback processes in
 4 stratiform mixed-phase clouds per- turbed by ship exhaust, *Geophys. Res. Lett.*, **44**, 1964–
 5 1972, <https://doi.org/10.1002/2016GL071358>, 2017.~~

6 Pruppacher, H. R., and Klett, J. D.: *Microphysics of Clouds and Precipitation*, 2nd ed., Kluwer,
 7 Dordrecht, Netherlands, 1997.

8 Shupe, M. D., and Intrieri, J. M.: Cloud radiative forcing of the Arctic surface: The influence
 9 of cloud properties, surface albedo, and solar zenith angle, *J. Climate*, **17**, 616–628, 2004.

10 Solomon, A., Feingold, G., and Shupe, M. D.: The role of ice nuclei recycling in the
 11 maintenance of cloud ice in Arctic mixed-phase stratocumulus, *Atmos. Chem. Phys.*, **15**,
 12 10631–10643, doi:10.5194/acp-15-10631-2015, 2015.

13 Stevens, B., and Feingold, G.: Untangling aerosol effects on clouds and precipitation in a
 14 buffered system, *Nature*, **461**, 607–613, 2009.

15 Stevens, B., Cotton, W., Feingold, G., and Moeng, C.: Large-eddy simulations of strongly
 16 precipitating, shallow, stratocumulus-topped boundary layers, *Journal of the Atmospheric
 17 Sciences*, **55**, 3616–3638, 1998.

18 ~~Stevens, R. G., Loewe, K., Dearden, C., Dimitrelos, A., Possner, A., Eirund, G. K.,
 19 Raatikainen, T., Hill, A. A., Shipway, B. J., Wilkinson, J., Romakkaniemi, S., Tonttila, J.,
 20 Laaksonen, A., Korhonen, H., Connolly, P., Lohmann, U., Hoose, C., Ekman, A. M. L.,
 21 Carslaw, K. S., and Field, P. R.: A model intercomparison of CCN-limited tenuous clouds
 22 in the high Arctic, *Atmos. Chem. Phys.*, **18**, 11041–11071, [https://doi.org/10.5194/acp-18-
 23 11041-2018](https://doi.org/10.5194/acp-18-11041-2018), 2018.~~

24 Sullivan, R. C., Miambres, L., DeMott, P. J., Prenni, A. J., Carrico, C. M., Levin, E. J. T.,
 25 and Kreidenweis, S. M.: Chemical processing does not always impair heterogeneous ice
 26 nucleation of mineral dust particles, *Geophys. Res. Lett.*, **37**, L24805,
 27 doi:10.1029/2010GL045540, 2010.

28 Tewari, M., Chen, F., Wang, W., Dudhia, J., LeMone, M. A., Mitchell, K., Ek, M., Gayno,
 29 G., Wegiel, J., and Cuenca, R. H.: Implementation and verification of the unified
 30 NOAA land surface model in the WRF model. *20th conference on weather analysis
 31 and forecasting/16th conference on numerical weather prediction*, pp. 11–15, 2004.

Deleted: ¶

Formatted: Font: Times New Roman, 12 pt

Formatted: Font: Times New Roman, 12 pt

Formatted: Justified, Indent: Left: 0", Hanging: 0.3", Space Before: 0 pt, After: 0 pt, Line spacing: 1.5 lines

Deleted: ¶

Formatted: Font: Times New Roman, 12 pt

Formatted: Font: Times New Roman, 12 pt

Formatted: Justified, Indent: Left: 0", Hanging: 0.3", Line spacing: 1.5 lines

- 1 Twomey, S.: Influence of pollution on shortwave albedo of clouds, *J. Atmos. Sci.* **34**, 1149–
2 1152, 1977.
- 3 Webb, E. K.: Profile relationships: The log-linear range, and extension to strong stability,
4 *Quart. J. Roy. Meteor. Soc.*, **96**, 67–90, 1970.
- 5 Wegener, A.: *Thermodynamik der Atmosphäre* (Leipzig, 1911).
- 6 Yamaguchi, T., and Feingold, G.: Technical note: Large-eddy simulation of cloudy boundary
7 layer with the Advanced Research WRF model, *J. Adv. Model. Earth Syst.*, **4**, M09003,
8 doi:10.1029/2012MS000164, 2012.
- 9 Zhang, T., Stamnes, K., and Bowling, S. A.: Impact of clouds on surface radiative fluxes and
10 snowmelt in the Arctic and Subarctic, *J. Climate.*, **9**, 2110-2123, 1996.

1 **9 Tables**

| Simulation Name | CCN Factor | INP Factor |
|------------------------------|-------------------|-------------------|
| --Constant Ice Runs-- | | |
| ConIce0.5 (red) | 1/2 | 1 |
| Control (black) | 1 | 1 |
| ConIce2.0 (blue) | 2 | 1 |
| --Linear Ice Runs-- | | |
| LinIce0.5 (red) | 1/2 | 1/2 |
| LinIce2.0 (blue) | 2 | 2 |
| FixCCN2.0 | 2 | 2 |

2 **Table 1:** Description of simulations completed and discussed in the paper.

1 **10 Figure Captions**

2 **Figure 1:** Measurements at Oliktok Point, Alaska 15-17 April 2015. (a) Ceilometer (black
3 dots) and Ka-band cloud radar reflectivity (colored shading). B) LWP and IWP, in units of gm^{-2} .
4 ². LW (c) and SW (d) surface radiation measurements, in units of Wm^{-2} . (e) Surface air
5 temperatures. (f) Surface wind direction, in units of degrees. (g) Surface wind speed, in units
6 of ms^{-1} . (h) Radiosondes at approximately 2330 UTC on 15 April, 1730 UTC and 2330 UTC
7 on 16 April, and 1830 UTC and 2330 UTC on 17 April.

8 **Figure 2:** Sounding measured at 0 UTC 17 April 2015 at Oliktok Point, Alaska. Left: water
9 vapor mixing ratio (q_v) and potential temperature (θ), in units of g kg^{-1} , and Kelvin
10 respectively. Right: zonal wind (U) and meridional wind (V), in units of m s^{-1} . The dashed
11 lines show the initial profiles used in the WRFLES experiments. The dashed line overlying
12 water vapor mixing ratio is the initial profile for the total water mixing ratio.

13 **Figure 3:** Time series from runs varying CCN concentrations with “constant” ice formation.
14 a) LWP, in units of gm^{-2} . b) IWP, in units of gm^{-2} . c) Scatterplot of minimum longwave heating
15 rate vs LWP, in units of K hour^{-1} and g m^{-2} , respectively. d) Scatterplot of integrated buoyancy
16 vs LWP, in units of m^3s^{-3} and g m^{-2} , respectively. For INP factors equal to 1.0 and CCN factors
17 2.0 (blue), 1.0 (black), and 0.5 (red).

18 **Figure 4:** Impact of increasing CCN by 2X (ConIce2.0 minus ConIce1.0) on (a) relative
19 humidity, (b) sublimation rate, (c) water vapor mixing ratio, and (d) temperature, in units of
20 percent, $\text{g m}^{-3} \text{s}^{-1}$, g kg^{-1} , $^{\circ}\text{C}$, respectively.

21 **Figure 5:** Time series from runs varying CCN concentrations with “constant” ice formation.
22 a) Maximum effective radius, in units of microns. b) Cloud mixed-layer liquid-ice water static
23 energy, in units Kelvin. c) Cloud base ice plus snow number concentration, in units of L^{-1} . d)
24 Vertically integrated net deposition rate, in units of $\text{g m}^{-2} \text{day}^{-1}$. For CCN factors 0.5 (red), 1.0
25 (black), and 2.0 (blue). For INP factors equal to 1.0 and CCN factors 0.5 (red), 1.0 (black), and
26 2.0 (blue).

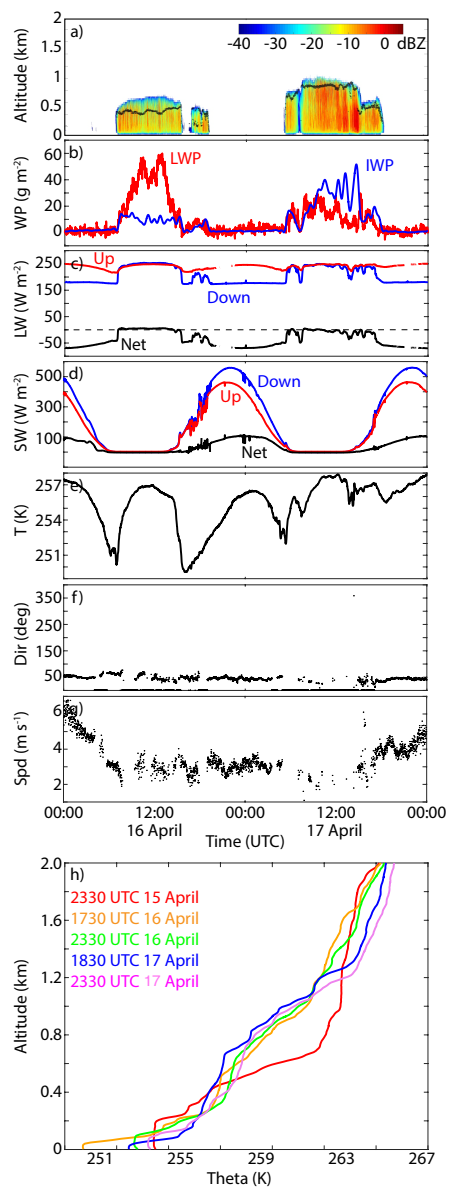
1 **Figure 6:** Time series from runs varying CCN concentrations with “linear” ice formation. a)
2 LWP, in units of gm^{-2} . b) IWP, in units of gm^{-2} . c) Liquid water fraction for ConIce (solid) and
3 LinIce (dashed). For CCN and INP factors 0.5 (red), 1.0 (black), and 2.0 (blue).

4 **Figure 7:** Time series from runs varying CCN concentrations with “linear” ice formation. a)
5 Maximum effective radius, in units of microns. b) Cloud mixed-layer liquid-ice water static
6 energy, in units Kelvin. c) Cloud base ice plus snow number concentration, in units of L^{-1} . d)
7 Vertically integrated net deposition rate, in units of $\text{g m}^{-2} \text{day}^{-1}$. For CCN and INP factors 0.5
8 (red), 1.0 (black), and 2.0 (blue).

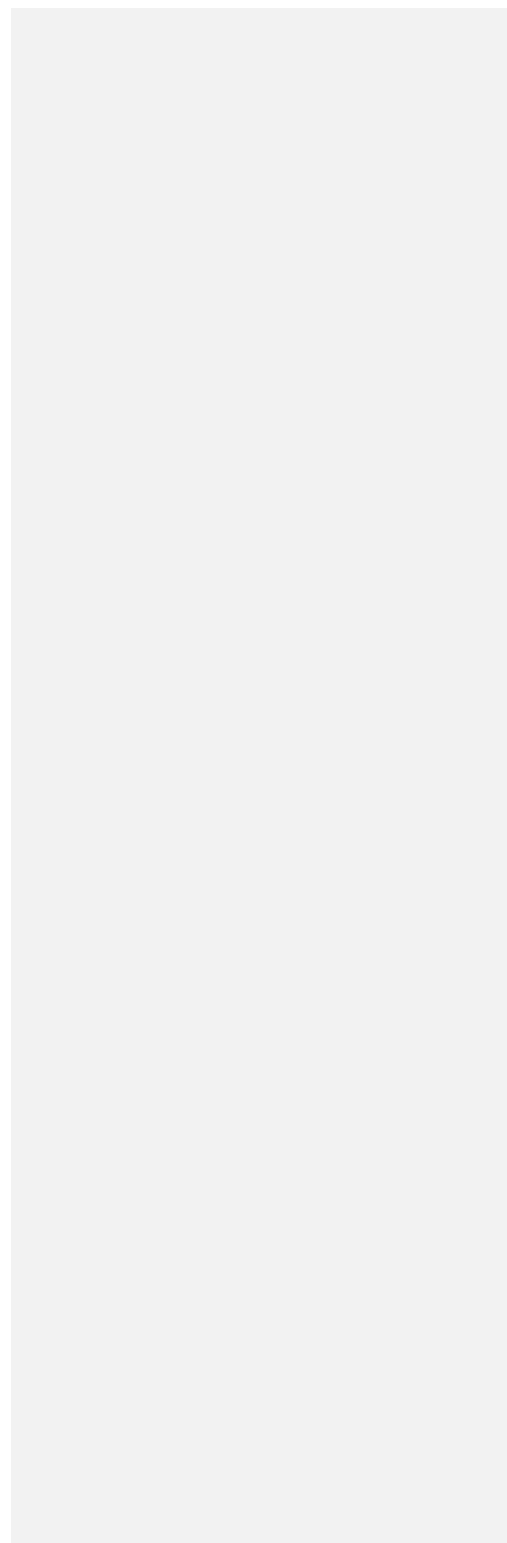
9 **Figure 8:** (a) CCN and (b) INP in “linear” ice runs at hour 10, in units of cm^{-3} and L^{-1} ,
10 respectively. For CCN and INP factors 0.5 (red), 1.0 (black), and 2.0 (blue).

11 **Figure 9:** Impact of prognostic CCN (LinIce2.0-FixCCN2.0) over hour 10. a) Droplet number
12 concentration (black) and snow mixing ratio (red), in units of cm^{-3} and $1.\text{e}^4 \text{g kg}^{-1}$,
13 respectively. b) Longwave radiative heating rate, in units of K hour^{-1} . c) Liquid water content,
14 in units of g m^{-3} . d) Buoyancy, in units of $\text{m}^2 \text{s}^{-3}$.

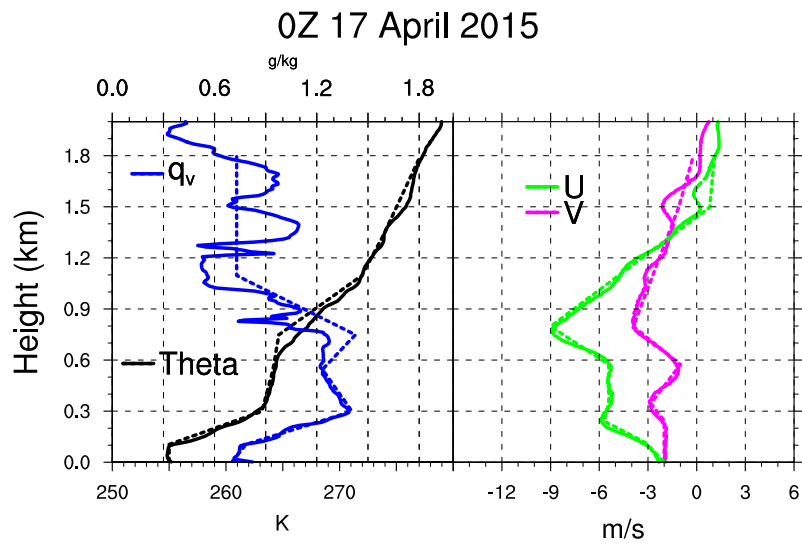
1



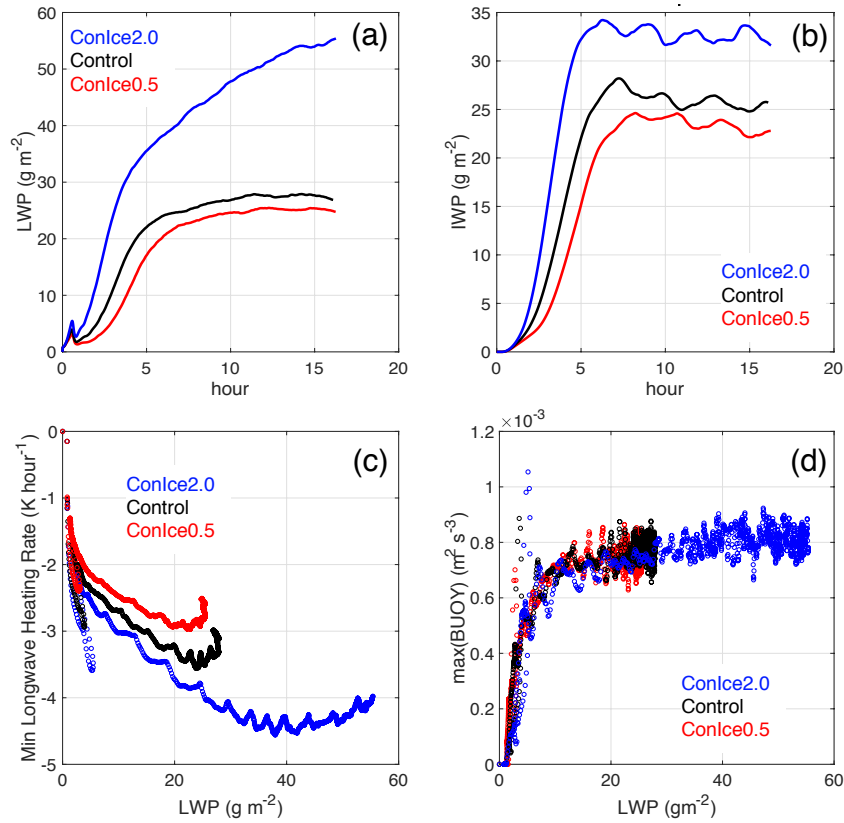
2



1 **Figure 1:** Measurements at Oliktok Point, Alaska 15-17 April 2015. (a) Ceilometer (black
2 dots) and Ka-band cloud radar reflectivity (colored shading). B) LWP and IWP, in units of gm^{-2} .
3 LW (c) and SW (d) surface radiation measurements, in units of Wm^{-2} . (e) Surface air
4 temperatures. (f) Surface wind direction, in units of degrees. (g) Surface wind speed, in units
5 of ms^{-1} . (h) Radiosondes at approximately 2330 UTC on 15 April, 1730 UTC and 2330 UTC
6 on 16 April, and 1830 UTC and 2330 UTC on 17 April.



1
 2 **Figure 2:** Sounding measured at 0 UTC 17 April 2015 at Oliktok Point, Alaska. Left: water
 3 vapor mixing ratio (q_v) and potential temperature (θ), in units of g kg^{-1} , and Kelvin
 4 respectively. Right: zonal wind (U) and meridional wind (V), in units of m s^{-1} . The dashed
 5 lines show the initial profiles used in the WRFLES experiments. The dashed line overlying
 6 water vapor mixing ratio is the initial profile for the total water mixing ratio.



1

2

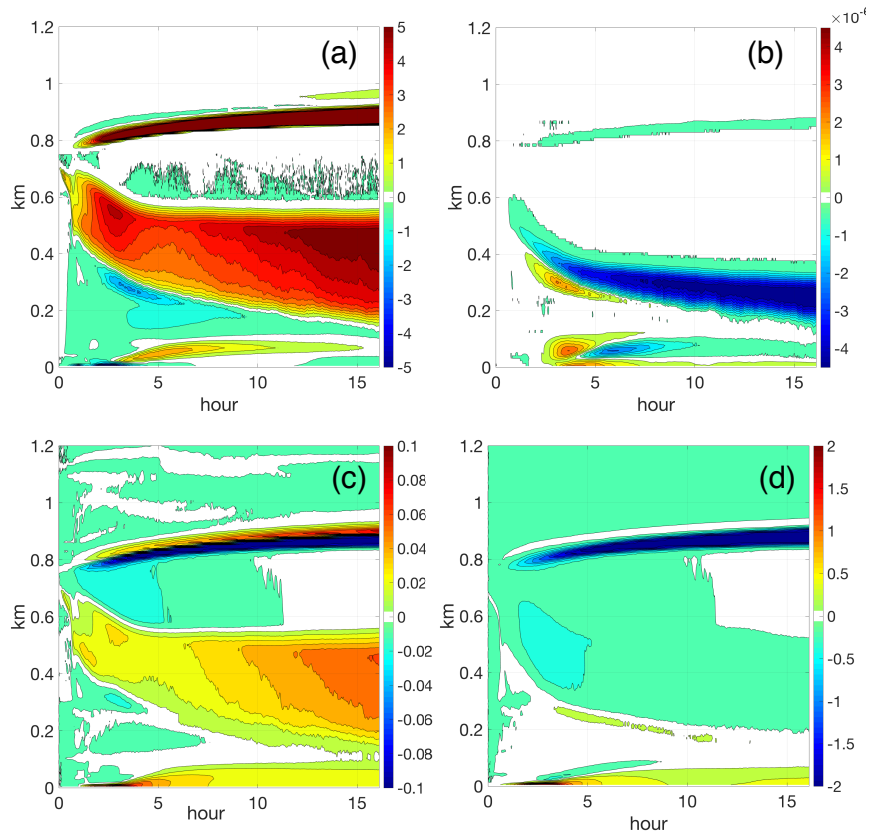
3 **Figure 3:** Time series from runs varying CCN concentrations with “constant” ice formation.

4 a) LWP, in units of gm⁻². b) IWP, in units of gm⁻². c) Scatterplot of minimum longwave heating

5 rate vs LWP, in units of K hour⁻¹ and g m⁻², respectively. d) Scatterplot of integrated buoyancy

6 vs LWP, in units of m³s⁻³ and g m⁻², respectively. For CCN factors 2.0 (blue), 1.0 (black), and

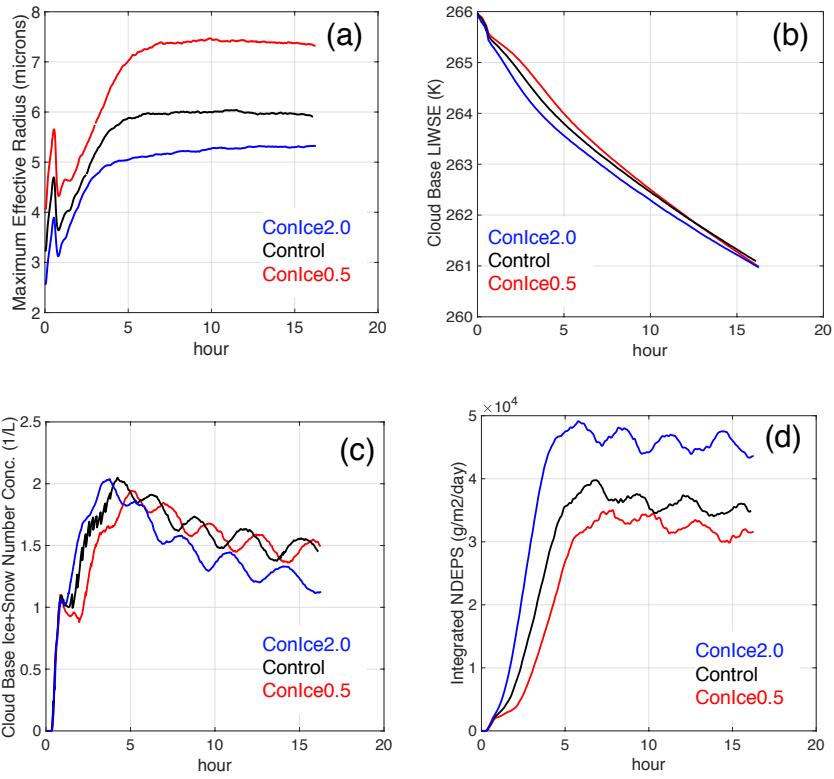
7 0.5 (red).



1

2

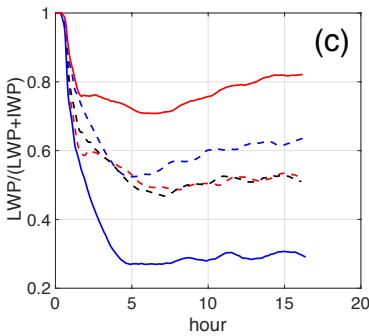
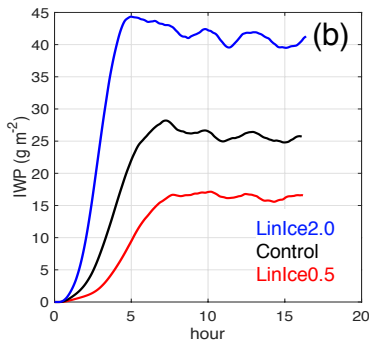
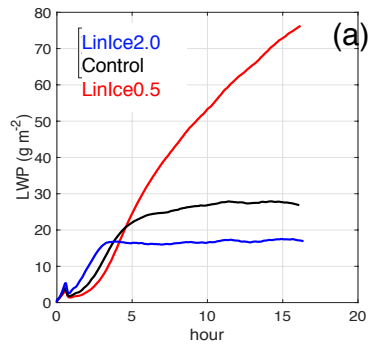
3 **Figure 4:** Impact of increasing CCN by 2X (ConIce2.0 minus ConIce1.0) on (a) relative
 4 humidity, (b) sublimation rate, (c) water vapor mixing ratio, and (d) temperature, in units of
 5 percent, $\text{g m}^{-3} \text{s}^{-1}$, g kg^{-1} , $^{\circ}\text{C}$, respectively.



1

2

3 **Figure 5:** Time series from runs varying CCN concentrations with "constant" ice formation.
 4 a) Maximum effective radius, in units of microns. b) Cloud mixed-layer liquid-ice water static
 5 energy, in units Kelvin. c) Cloud base ice plus snow number concentration, in units of L⁻¹. d)
 6 Vertically integrated net deposition rate, in units of g m⁻² day⁻¹. For CCN factors 0.5 (red), 1.0
 7 (black), and 2.0 (blue).

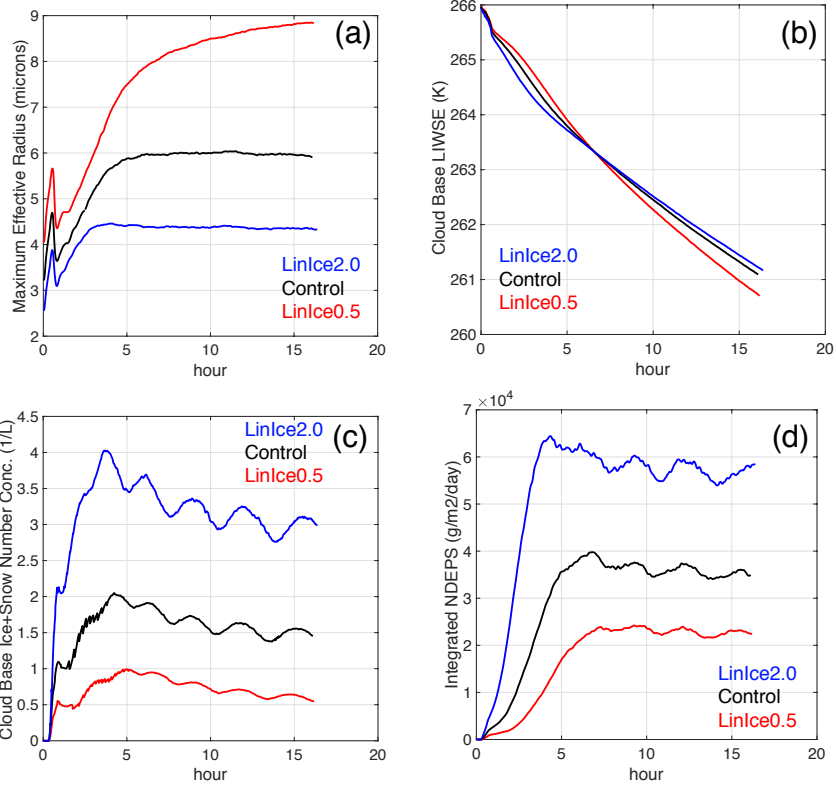


1

2

3

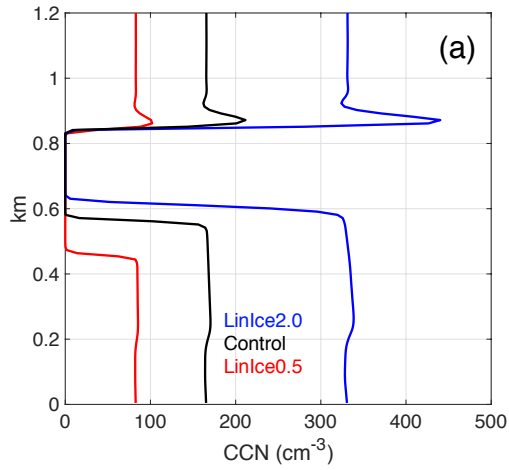
4 **Figure 6:** Time series from runs varying CCN concentrations with “linear” ice formation. a)
 5 LWP, in units of g m^{-2} . b) IWP, in units of g m^{-2} . c) Liquid water fraction for ConIce (dashed)
 6 and LinIce (solid). For CCN and INP factors 0.5 (red), 1.0 (black), and 2.0 (blue).



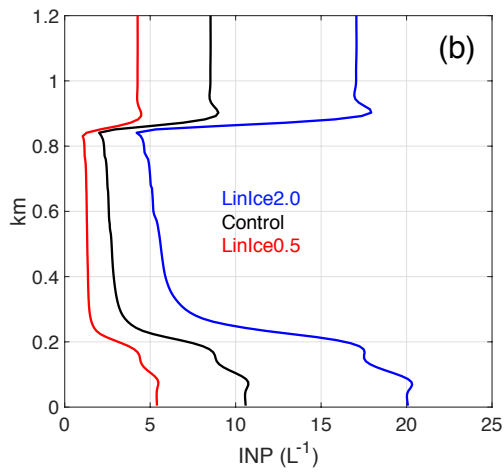
1

2

3 **Figure 7:** Time series from runs varying CCN concentrations with “linear” ice formation. a)
 4 Maximum effective radius, in units of microns. b) Cloud mixed-layer liquid-ice water static
 5 energy, in units Kelvin. c) Cloud base ice plus snow number concentration, in units of L^{-1} . d)
 6 Vertically integrated net deposition rate, in units of $g\ m^{-2}\ day^{-1}$. For CCN and INP factors 0.5
 7 (red), 1.0 (black), and 2.0 (blue).

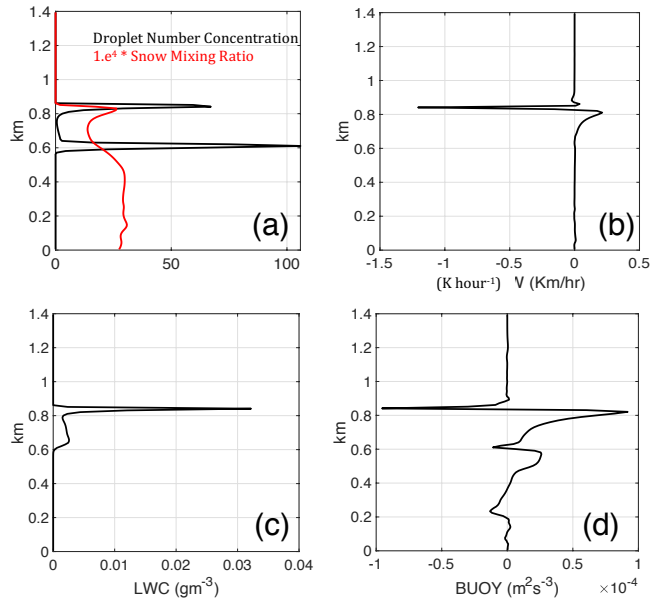


1



2

3 **Figure 8:** (a) CCN and (b) INP in “linear” ice runs at hour 10, in units of cm^{-3} and L^{-1} ,
 4 respectively. For CCN and INP factors 0.5 (red), 1.0 (black), and 2.0 (blue).



1

2

3

4 **Figure 9:** Impact of prognostic CCN (LinIce2.0-FixCCN2.0) over hour 10. a) Droplet
 5 number concentration (black) and snow mixing ratio (red), in units of cm^{-3} and $1.e^4 * \text{g kg}^{-1}$,
 6 respectively. b) Longwave radiative heating rate, in units of K hour^{-1} . c) Liquid water
 7 content, in units of g m^{-3} . d) Buoyancy, in units of $\text{m}^2 \text{s}^{-3}$.